Environmental Science & Technology

pubs.acs.org/est

Article

Hydrocarbon Tracers Suggest Methane Emissions from Fossil Sources Occur Predominately Before Gas Processing and That Petroleum Plays Are a Significant Source

Ariana L. Tribby, Justin S. Bois, Stephen A. Montzka, Elliot L. Atlas, Isaac Vimont, Xin Lan, Pieter P. Tans, James W. Elkins, Donald R. Blake, and Paul O. Wennberg*

Cite This: *Environ. Sci. Technol.* 2022, 56, 9623−9631

Read Online

ACCESS | Metrics & More | Article Recommendations | Supporting Information

ABSTRACT: We use global airborne observations of propane (C_3H_8) and ethane (C_2H_6) from the Atmospheric Tomography (ATom) and HIAPER Pole-to-Pole Observations (HIPPO), as well as U.S.-based aircraft and tower observations by NOAA and from the NCAR FRAPPE campaign as tracers for emissions from oil and gas operations. To simulate global mole fraction fields for these gases, we update the default emissions' configuration of C_3H_8 used by the global chemical transport model, GEOS-Chem v13.0.0, using a scaled C_2H_6 spatial proxy. With the updated emissions, simulations of both C_3H_8 and C_2H_6 using GEOS-Chem are in reasonable agreement with ATom and HIPPO observations, though the updated emission fields underestimate C_3H_8 accumulation in the arctic wintertime, pointing to additional sources of this gas in the high latitudes (e.g., Europe). Using a Bayesian hierarchical model, we estimate global emissions of C_2H_6 and C_3H_8 from fossil fuel production in 2016−2018 to be 13.3 ± 0.7 (95% CI) and 14.7 ± 0.8 (95% CI) Tg/year, respectively. We calculate bottom-up hydrocarbon emission ratios using basin composition measurements weighted by gas production and find their magnitude is higher than expected and is similar to ratios informed by our revised alkane emissions. This suggests that emissions are dominated by pre-processing activities in oil-producing basins.

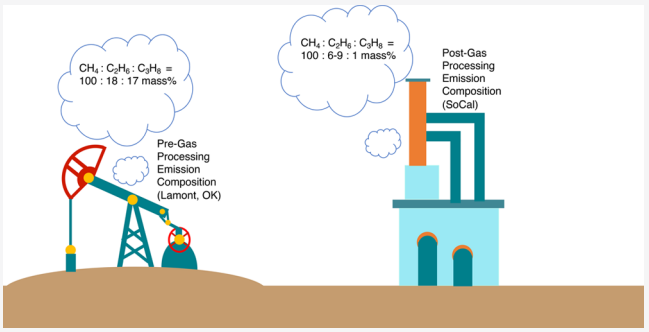

KEYWORDS: *ethane, propane, natural gas, methane, energy*

INTRODUCTION

Many studies have diagnosed recent methane (CH_4) trends (both global and regional) using ethane (C_2H_6) atmospheric ratio signatures. However, the rejection of C_2H_6 by oil and gas producers (in the U.S., and presumably in countries following similar economic trends, Figure S1) results in an increase in the mole fraction of C_2H_6 in the natural gas pipelines. Thus, to the extent that losses occur in the pipelines and at the end users of natural gas, emissions of C_2H_6 may not necessarily directly reflect CH_4 emissions, adding additional uncertainty in CH_4 emission estimates from natural gas operations. In addition, a global uptick in hydraulic fracturing has shifted production from dry to wet fields, resulting in an increase in the ratios of both C_2H_6 and C_3H_8 to CH_4,[1] further complicating the use of the alkanes to diagnose the underlying CH_4 emission sources.[2−4]

Given the uncertainty in using C_2H_6 alone as a tracer for CH_4 emissions, we use both C_2H_6 and propane (C_3H_8) to diagnose whether significant CH_4 emissions from natural gas and petroleum occur before gas processing. Unlike C_2H_6, C_3H_8 has a much higher market value and therefore does not undergo "rejection".[5] Provided downstream losses are minimal and the raw gas ratio of C_3H_8 to CH_4 is known, C_3H_8 can provide a constraint for CH_4 emissions from raw, unprocessed natural gas.

In this study, we employ global observations from aircraft, including the 2009−2011 High-Performance Instrumented Airborne Platform for Environmental Research (HIAPER) Pole-to-Pole Observations (HIPPO)[6] and the 2016−2018 Atmospheric Tomography (ATom)[7] missions, which provide vertical profiles of a variety of constituents, including C_2H_6 and C_3H_8, around the remote atmospheres of the globe. Together with the large-scale chemical transport model GEOS-Chem, we estimate global fossil emissions of C_2H_6 and C_3H_8.

Received: February 11, 2022
Revised: May 18, 2022
Accepted: May 18, 2022
Published: June 14, 2022

MATERIALS AND METHODS

Observations from the National Oceanic and Atmospheric Administration (NOAA) Global Monitoring Laboratory (GML). Measurements of CH_4,[8−10] C_2H_6, and C_3H_8[11] from flask air collected by the NOAA GML tower[12] and aircraft[13] near oil/natural gas basins were used as unprocessed gas references. We refer to site locations using state abbreviations. More information on data processing/spatial coverage is included in section S2, Table S1, and Figure S5. To better quantify geophysical variability and generate a confidence interval in the correlation between C_2H_6 and C_3H_8 mole fractions, we implement a pairs bootstrap to generate replicates of C_2H_6 and C_3H_8 observations. The CIs calculated from the bootstrapped samples are much broader than those calculated assuming the noise in the measurements is dominated by analytical errors. This suggests that geophysical noise induced by differences in transport and chemistry dominates the statistics. See section S2.1 for more details.

FRAPPE Observations. FRAPPE C130 flight data were taken within the Colorado Front Range between July 26 and August 19, 2014. We accessed the data on October 6, 2021 from www.air.larc.nasa.gov from the WAS C130 merge file. Our data processing for FRAPPE is similar to our methods for the NOAA in situ samples. A spatial illustration of FRAPPE observations is shown in Figure S6.

HIAPER Pole-to-Pole Observations and ATmospheric Tomography Data. The HIPPO campaign was a sequence of five global measurement campaigns which sampled from near the North Pole to the coastal waters of Antarctica, covering different seasons between 2009 and 2011. Similarly, ATom took place from 2016 and 2018. Flight paths of HIPPO and ATom campaigns are illustrated in Figure S22, and specific details about the data sources are included in section 3 of the Supporting Information (SI).

Only data observed at >20° north were used since the majority of emissions of these short-lived gases of interest lie in the northern hemisphere. The lifetime of C_3H_8 and C_2H_6 are on the order of a few months or shorter during the summer, and the time it takes for mixing between the northern to southern hemispheres is on the order of a year,[14] so the mole fraction of these gases of interest is very low in the southern hemisphere.

Because C_2H_6 and C_3H_8 are relatively short-lived gases, their abundance in the stratosphere is low and poorly connected to the underlying fluxes. To exclude stratospheric observations, we use N_2O (Panther/UCATS instrument), which is inert and generally well-mixed in the troposphere but is destroyed in the stratosphere by photolysis and reaction with O^1D.[15] Thus, we exclude from our analysis data with low N_2O mole fraction (Figure S23).

As our focus in this analysis is quantifying the global emissions of these gases, we exclude from our analysis data where local fluxes substantially influence the mole fraction of these alkanes. We use a simple land and altitude constraint and HCN as a tracer to remove plumes from highly local sources (including both energy infrastructure and wildfires, Figures S24−S26). We also exclude regions and times where the lifetime of the alkanes is very short and thus regional/local sources dominate the variance. Thus, we do not analyze the aircraft summer data (results for the summer are shown in the SI) or data in the subtropics, where the alkane distribution is very sensitive to transport from the extratropics where most emissions of C_2H_6 and C_3H_8 originate. To exclude subtropical air, we only analyze measurements with tropopause pressure above 100 hPa (about 5% of the data were excluded under this constraint) for both ATom and HIPPO, which was sufficient to reduce the influence of tropical intrusions. See Table S2 for a comprehensive outline of the filters we use.

As in other studies,[16,17] we use potential temperature (θ, in units of Kelvin) in our analysis as a zonal coordinate. Potential temperature is conserved following adiabatic flow, and in the extratropics, variability within large-scale circulation can be well captured using this coordinate system. As a result, trace gases that have long lifetimes compared to synoptic-scale meteorology, which has a horizontal length scale on an order of 1000 km or more and a time scale of about 10 days,[14,18] will be well correlated with θ. Using θ as a dynamical coordinate allows us to more accurately compare low spatial resolution GEOS-Chem simulations with the aircraft in situ measurements (compared with simply using altitude and latitude coordinates, Figure S27). Potential temperature is not well-correlated with trace gases in the tropics or boundary layer, where moist convection and surface-drag-driven turbulence can result in nonunique pairs or when the photochemical lifetimes are short (summer).

GEOS-Chem Simulations. We simulated HIPPO and ATom measurements using the GEOS-Chem "classic" global 3-D chemical transport model with default settings (details about the simulations and emissions are provided in the SI, section 4). We use the same constraints as the aircraft observations, except we use a boundary layer height parameter. As described below, we use a Bayesian model to provide a best estimate for global emissions of C_2H_6 and C_3H_8 and their uncertainty. One contribution to the error estimate is transport errors in GEOS-Chem. To capture some of the uncertainty in the transport field, we sample the GEOS-Chem model several days before and after the in situ sampling time along the aircraft flight path, which we refer to as "synoptic replicates". Finally, all GEOS-Chem simulations of C_3H_8 and C_2H_6 were interpolated on the vertical coordinate using θ to the aircraft measurements. As expected, GEOS-Chem synoptic replicates show less consistency in latitude (Figure S27), providing support for using θ as an analysis coordinate.

Bayesian Inference. We wish to quantify the global emissions of C_3H_8 and C_2H_6 using the observed mole fraction of these alkanes during ATom and HIPPO. The ambient mole fraction of C_3H_8 and C_2H_6 is most sensitive to their total northern hemisphere emissions during the winter/fall/spring when there is decreased sunlight/oxidation. As such, we assume differences between the GEOS-Chem simulations and the aircraft observations can be largely attributed to the underlying emissions grid, such that

$$a = \mathrm{gcs}\cdot\alpha \tag{1}$$

where a is the aircraft C_2H_6 or C_3H_8 mole fraction, gcs is the GEOS-Chem simulation of C_2H_6 or C_3H_8 mole fraction, and α is a scalar that represents the missing emissions of C_3H_8 and C_2H_6 from default emissions. We developed a Bayesian hierarchical model to estimate the missing emissions, where eq 1 forms the basis of our model. Our model only uses the GEOS-Chem simulated alkane mole fraction data (synoptic replicates), the alkane mole fractions observed by the aircraft, tropopause height, and UTC time. Our complete statistical model and its development, priors (Figures S37−S41), as well as the software used, are included in the SI, section 5.

https://doi.org/10.1021/acs.est.2c00927
Environ. Sci. Technol. 2022, 56, 9623−9631

Hydrocarbon Percent Composition Literature Compilation and Bootstrapping. We gather literature measurements of hydrocarbon composition from unprocessed gas from oil- and gas-producing basins in the U.S. and around the globe to calculate emission ratios. Summary statistics of the percent composition by region and the corresponding literature source is included in Tables S4 and S5 (SI). Gas composition varies significantly across basins, so we perform bootstrap calculations for data samples within each basin separately. For each basin, we draw random pairs of hydrocarbon composition measurements (CH_4, C_2H_6, and C_3H_8) for the size of the data set and then take the mean and repeat this 10,000 times. We use these bootstrap samples in subsequent calculations (eq 2) to arrive at emission ratios (Figure 6).

RESULTS AND DISCUSSION

CH_4 Leaks from U.S. Energy Activities Are Dominated by Emissions from Unprocessed Natural Gas. C_3H_8 and C_2H_6 are highly correlated at the NOAA sites (Figure 1). The

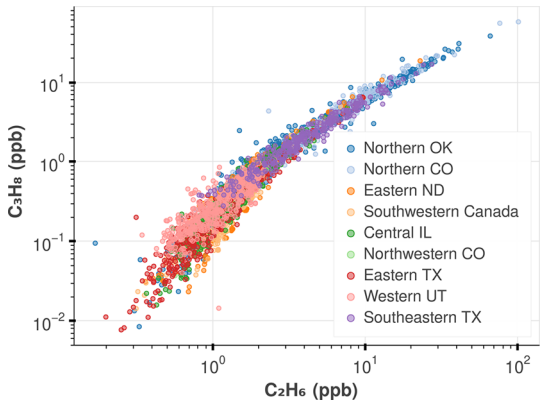

Figure 1. Measurements of C_2H_6 and C_3H_8 from ongoing NOAA GML tower and aircraft sites (Table S1) from 2005 to 2018. The data follow the photochemical aging distribution described in Parrish et al., where the data below 1 ppb C_3H_8 are affected by photochemically aged emissions and mixing processes. As such, we only study the ratio of these gases in the 50th highest percentile (everything above 1 ppb C_3H_8) that would indicate fresh emissions. After this filtering, two sites, Northwestern CO and Western UT (site codes NWR and UTA), did not have any data in the fresh emission regime and are not included in further analysis (more detail in Figure S8).

data shown were obtained across 2−11 years and include tower and aircraft data (Table S1). The cross plot of C_3H_8 and C_2H_6 illustrates two distinct chemical regimes, similar to those described by Parrish et al.[19] Above 1 ppb C_3H_8, the distribution is nearly linear, consistent with the mixing of fresh non-photochemically aged emissions into the background atmosphere. At mole fractions below 1 ppb, a second regime is defined by mixing of the aged emissions (the lifetime of C_3H_8 is much less than that of C_2H_6). To explore the characteristics of unprocessed natural gas emissions, we study the ratio of these gases within the 50th highest percentile of C_3H_8 for the combined sites. Varying this demarcation ±10% negligibly affects the linear fit (Figure S10). We find that the ratio of C_3H_8 to C_2H_6 in the linear regime to be [0.63, 0.70] (ppb/ppb, 95% CI), and FRAPPE observations show a similar trend at [0.76, 0.87] (Figure S9).

Within the fresh emission chemical regime, the NOAA C_3H_8/C_2H_6 ratio changes minimally before and after 2012 ([0.62, 0.67] and [0.63, 0.71], respectively, ppb/ppb 95% CI, Figure S9) and over the entire time series (Figure S19). An unchanging C_3H_8/C_2H_6 ratio over time across the U.S. despite large changes in the C_3H_8/C_2H_6 ratio in processed gas during the same years (Figure S1) suggests that the majority of the alkane (and likely CH_4) emissions occur before the gas processing stage. (During gas processing, most of the C_3H_8 and sometimes much of the C_2H_6 are separated from the raw gas.) Conversely, post-processing (pipeline) composition of C_2H_6 at Playa del Rey in Southern California follows rejection trends, where the C_3H_8/C_2H_6 ratio has decreased by 8% from 2008 to 2018 and in recent years is about 18% lower in magnitude compared to the NOAA ratio (Figure S4). (Processed gas in California is a good representation of typical gas composition of domestic and globally imported consumer-grade gas.[20]) Our results are in agreement with Rutherford et al.'s U.S.-based model for CH_4 emissions, which finds that unintentional emissions from the production segment (namely, liquid storage tanks and other equipment leaks) are the largest contributors to divergence with the EPA's GHGI.[21]

We use the same chemical aging approach to construct a background for NOAA and FRAPPE CH_4 observations (Figures S7 and S11). Since we only focus on the linear part of the chemical aging distribution, our analysis is not terribly sensitive to how the CH_4 anomaly is determined (it simply produces varying intercepts, Figure S10). Consistent with the analysis of Lan et al.[2] (see Figures S20 and S21), the ratio of C_3H_8 and C_2H_6 to CH_4 has increased with time, reflecting a growing importance of oil exploration on CH_4 emissions in the U.S.

C_3H_8 is demonstrated to be a useful tracer that constrains oil- and gas-related CH_4 emissions. Given that the fit of C_3H_8 versus CH_4 (and C_2H_6 versus CH_4) have similar precision over the whole record, using C_3H_8 as a tracer likely separated nearby competing non-oil and gas CH_4 emissions. However, if there were to be non-oil and gas CH_4 emissions that were spatially coherent to the NOAA observation sites, our C_3H_8 versus CH_4 and C_2H_6 versus CH_4 emission ratios would be impacted. Investigating and potentially separating spatially coherent emissions of nonfossil origins would be the topic of future studies.

NOAA observations at Oklahoma ARM site are especially impacted by nearby unprocessed gas emissions, as C_2H_6 and C_3H_8 correlations with CH_4 have less noise compared to other sites (Figures S12 and S13). While the ratios of C_3H_8 and C_2H_6 versus CH_4 have increased by 50% at NOAA Oklahoma site since 2010, we find that both C_2H_6 and C_3H_8 versus CH_4 ratios are fractionally increasing at the same rate (Figure 2). That the atmospheric C_2H_6 and C_3H_8 increase fractionally the same suggests that the ratio of the alkanes in the reservoirs producing these emissions do not change significantly over the time of this record. Below, we use the 2017 average C_3H_8/CH_4 and C_2H_6/CH_4 from NOAA Oklahoma site ([0.060, 0.061] and [0.086, 0.088] ppb/ppb, respectively, Figure S21) to compare to ratios between our emission estimates for C_3H_8 and C_2H_6 to published estimates of CH_4 emissions from oil and gas exploration.

Default GEOS-Chem Simulations Underestimate C_3H_8 Compared to Aircraft Observations. We compare the cross plot of C_3H_8 to C_2H_6 from the HIPPO and ATom aircraft measurements and GEOS-Chem simulations to the NOAA measurements (Figure 3). As expected, both the aircraft observations and GEOS-Chem simulations fall under

https://doi.org/10.1021/acs.est.2c00927
Environ. Sci. Technol. 2022, 56, 9623−9631

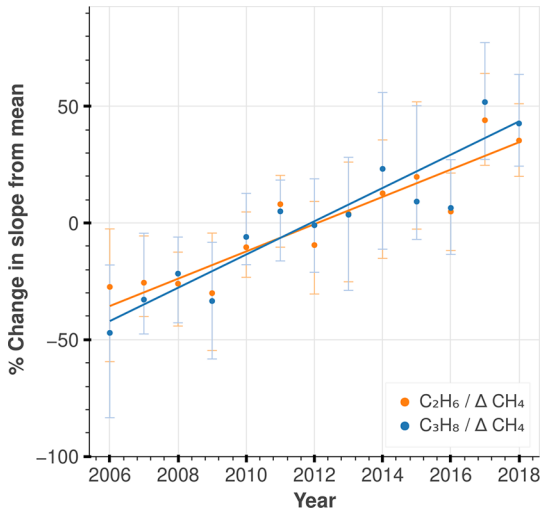

Figure 2. Yearly correlation between NOAA hydrocarbon versus CH_4 anomaly in Oklahoma. We show the percent change of anomalies/year with respect to the mean hydrocarbon and methane anomalies. The trend for C_3H_8/CH_4 is 7.13 ± 1.44% with an R^2 of 0.71. The trend for C_2H_6/CH_4 is 5.87 ± 1.26% with an R^2 = 0.69. The variability in the trend comes from the standard error of a linear regression. The variability in the individual points comes from the 95% confidence interval of a pairs bootstrap of the alkanes and CH_4 anomalies. (We ran a pairs bootstrap for co-measurements of C_3H_8 and ΔCH_4 and compute the slope of the correlation for each bootstrap sample and repeated this for every year in the data; please see the Materials and Methods section.) This trend in units of ppt/ppb/year is shown in Figure S21.

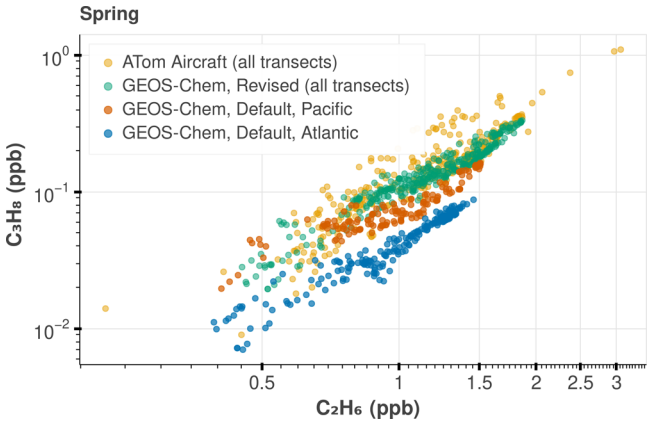

Figure 4. Impact of revised C_3H_8 emissions on GEOS-Chem simulation. Combined Pacific and Atlantic transects for ATom 4 aircraft campaign, which took place during Spring 2018, are shown in gold. The GEOS-Chem simulation using default C_3H_8 emissions are shown in blue and orange, referring to the Pacific and Atlantic transects, respectively. The GEOS-Chem simulation after implementing the revised C_3H_8 emissions is shown in green. The rest of the ATom and HIPPO campaigns are shown in Figures S35 and S36.

the photochemically aged emissions part of the NOAA distribution. While the aircraft data overlay the NOAA measurements almost perfectly (especially in the winter when the lifetimes of both gases are the longest), GEOS-Chem underestimates C_3H_8, particularly over the Atlantic curtain (Figures 3 and 4). The same conclusion is drawn for HIPPO time periods (Figures S31, S32, and S34). Because the atmospheric lifetimes of C_3H_8 and C_2H_6 are different and vary seasonally due to the much higher concentrations of OH in the summer, our estimate of global C_2H_6 and C_3H_8 emissions from GEOS-Chem comparisons are sensitive to the a priori spatial distribution of these emissions.

Relative to C_2H_6, the default GEOS-Chem v13.0.0 C_3H_8 emissions result in a much larger underestimate of C_3H_8 mole fractions over the Atlantic transect compared to the Pacific (Figures 3 and 4), implying an underestimate over North America. This pattern is most clearly visible in the summer when the C_3H_8 lifetime is short. In contrast, the default C_2H_6 emissions produce a good simulation of the ATom data (within 5%) over both ocean basins (Figures 3 and 4). As such, we use the mean ratio observed in the linear regime of the NOAA data (0.67 C_3H_8/C_2H_6, ppb/ppb Figure S9) as the default global ratio of their emissions to update GEOS-Chem. In mass units (as used in the GEOS-Chem emissions), this is ≈0.99 kg C_3H_8/kg C_2H_6. Given the remarkable coherence in both the large-scale fields from the aircraft over both the Atlantic and Pacific transects and in the NOAA data, the spatial distribution of the emissions ratios for both gases must be very similar upwind of the Pacific (e.g., Asia) and the

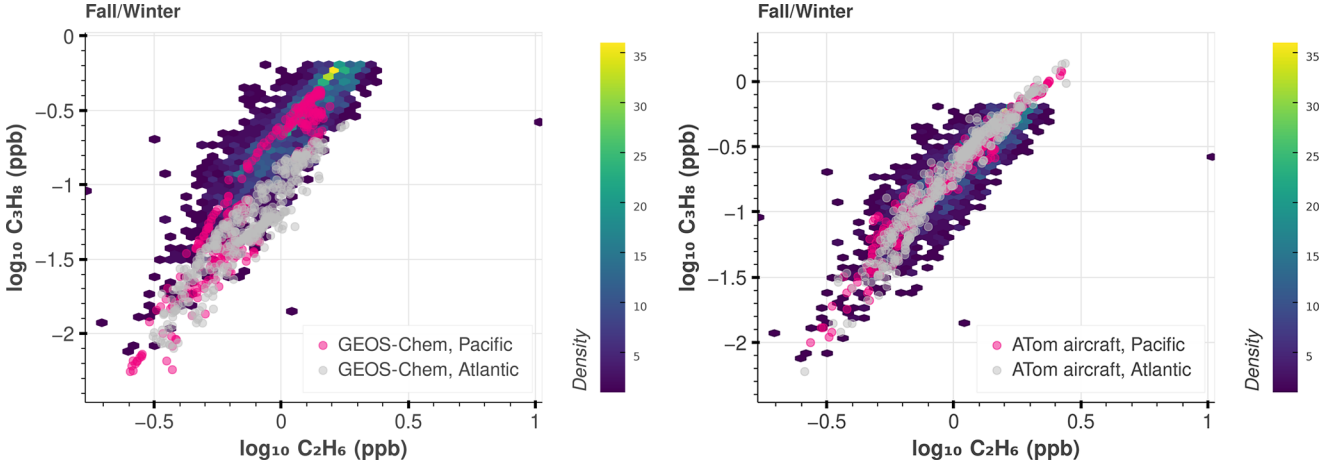

Figure 3. Comparison of C_3H_8 versus C_2H_6 for NOAA, ATom aircraft, and GEOS-Chem simulations during fall/winter seasons. NOAA photochemically aged measurements (all sites, 2005−2018), as explained in the text, are shown on the heat map (colored by the number density of data). The spring/summer seasons are included in Figures S29, S30, and S33. HIPPO is shown in Figure S34.

https://doi.org/10.1021/acs.est.2c00927
Environ. Sci. Technol. 2022, 56, 9623−9631

Atlantic (North America). As such, in our revised emission fields for C_3H_8, we simply used the default C_2H_6 emissions configuration used by GEOS-Chem v13.0.0. This scaling substantially altered the spatial distribution of C_3H_8 emissions (Figure S28). The effect on the C_3H_8 simulation is shown in Figure 4 using ATom 4 as an example, where updating the emissions resulted in a much better agreement between GEOS-Chem C_3H_8 and aircraft measurements (other campaigns are included in Figures S35 and S36). Although simulations are greatly improved using the revised emissions, it appears there is a missing high latitude source of C_3H_8 and C_2H_6 (Figures S47, S48, S54, and S55).

Bayesian Model Suggests Decadal Increase in Global C_2H_6 and C_3H_8 Anthropogenic Fossil Emissions. The results of our Bayesian inference were satisfactory. We had good sampling of our posterior, and the sampling diagnostics were excellent (Figures S43, S44, S50, and S51). We performed tests that verified our inference procedure could capture the ground truth (using simulated data for which the ground truth is known), and that our posterior was more concentrated around the ground truth than the prior (Figure S42). Furthermore, our model could generate the measured data reasonably well; the majority of the measured aircraft data fell into the 30th and 50th percentile of the simulated Bayesian model data (Figures S47, S48, S54, and S55). The exception to this was the summer season, where the Bayesian model does not capture the measured aircraft data well. This is expected, since during the summer we do not observe a robust relationship between potential temperature and C_3H_8 or C_2H_6. The model remained robust even when varying the sensitivity to low mole fractions of alkanes with tropical origin (Figures S58–S60).

During ATom 2 (winter) Atlantic curtain, the GEOS-Chem simulations poorly capture the observed C_2H_6 and C_3H_8 at low potential temperature compared to the aircraft. These measurements are samples obtained at low altitude, high latitude, and cold temperatures (Figure S49). During the winter, these arctic airmasses are often characterized by stagnant conditions, with less mixing with the midlatitudes.[22] As a result, emissions that occur at high latitudes during the winter can be trapped there unless the zonal flow is disrupted. Additionally, emissions of C_2H_6 and C_3H_8 near the arctic during the winter will oxidize more slowly relative to midlatitudes due to the cold temperature and minimal sunlight. These conditions result in high C_2H_6 and C_3H_8 mole fraction over the arctic relative to remote midlatitude chemical regimes. The measurements subject to arctic conditions during ATom were too few to make a substantial impact on the overall Bayesian emission estimates, but during HIPPO winter flights, few samples were obtained, resulting in a large bias toward arctic data. We place much more weight on the ATom winter C_3H_8 analysis estimate of global C_3H_8 emissions since the arctic represents only a small fraction of the atmosphere.

It is likely that GEOS-Chem v13.0.0 is missing a high latitude emissions source (Figures S47–S49, S54, and S55). Underestimation of C_3H_8 and C_2H_6 at high latitudes is consistent with other studies, which found that fossil fuel emissions from Eurasia accounted for the largest underestimation.[23] It is possible that emissions from northern Europe may account for this discrepancy, as fossil emissions were found to be underestimated,[23] and our revised C_3H_8 emissions decreased in that region after implementing the emission C_2H_6 proxy (Figure S28). This, combined with a relatively lower number of HIPPO aircraft observations at lower latitudes, results in a substantial positive bias on the overall Bayesian emissions estimate for C_3H_8 during winter 2009 (Figure S62).

We report our Bayesian estimates for each seasonal campaign and ocean transect during 2009–2011 and 2016–2018 and what the GEOS-Chem v13.0.0 default emissions grids should be scaled by, according to our analysis (Figures S45, S46, S52, and S53 and SI section 5.8). We estimate global emissions of C_2H_6 and C_3H_8 from fossil fuel production from 2016 to 2018 to be 13.3 ± 0.7 (95% CI) and 14.7 ± 0.8 (95% CI) Tg/year, respectively. Our results compare well to other studies (Figure 5 and Figure S62). Our estimates suggest

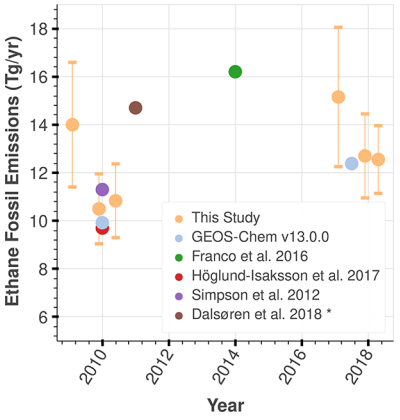

Figure 5. Global revised ethane anthropogenic fossil emissions compared to other studies. Our emissions estimate in 2016–2018 (during ATom) and 2009–2011 (during HIPPO) includes our revised emissions for winter, fall, and spring seasons that we determined with our Bayesian model during each season. As discussed in the text, fewer samples were obtained during HIPPO, resulting in a sampling bias that we test by restricting observations and simulations to ±300 K potential temperature (Figures S56 and S57). This test affects the estimate about ±1 Tg during 2010–2011 but affects our estimate by up to 12 Tg in 2009. We compare our revised emissions to the default emissions from GEOS-Chem v13.0.0. The studies included here[23,25−27] represent anthropogenic fossil emissions, except for the work by Dalsøren et al., which also includes biofuel, agriculture, and waste. We obtained the CEDS CMIP6 estimate from Dalsøren et al. Our emissions estimates do not include biomass burning or biofuels. Propane emissions are included in Figure S62.

emissions of C_2H_6 have increased by about 15% from 2010 to 2017 when comparing the mean revised C_2H_6 emissions during those time periods (Figure S61). Emissions of C_3H_8 are calculated to have increased more (65%, Figure S62), but this estimate is highly uncertain due to the few samples obtained during HIPPO and the impact of the Arctic winter pooling in both campaigns. Nevertheless, these increases are consistent with greater oil production emissions contribution. Similarly, Helmig et al., which used data from a global surface network and atmospheric column observations, found about a 22% increase in C_2H_6 emissions between 2009 and 2014.[24]

Oil Exploration Plays a More Significant Role in Global CH_4 Compared to Dry Gas. We calculate an emission ratio of C_3H_8/CH_4 for n basins or countries using the following equation:

$$E\left(\frac{C_3}{C_1}\right) = \sum_{i=1}^{n}\left(\left(\frac{P_{\mathrm{DNG}_i} \times {}^{C_{1i}}/_{\mathrm{tot}_i}}{P_{\mathrm{DNG}} \times {}^{C_1}/_{\mathrm{tot}}}\right)\left(\frac{C_{3i}}{C_{1i}}\right)\right) \quad (2)$$

https://doi.org/10.1021/acs.est.2c00927
Environ. Sci. Technol. 2022, 56, 9623−9631

where P_{DNG} is the dry natural gas production (in million tonnes), C_1 and C_3 are the bootstrapped samples of measured hydrocarbon fractions in raw natural gas samples (in mass%, details on the bootstrapping in the Materials and Methods section), and tot is the sum of the bootstrapped samples of measured hydrocarbon fractions for CH_4, C_2H_6, and C_3H_8. (Note that our $E\left(\frac{C_3}{C_1}\right)$ emission ratios are inherently weighted by natural gas production by basin, P_{DNG}.) $E\left(\frac{C_2}{C_1}\right)$ is calculated similarly. We refer to the emission ratio in eq 2 as the "literature" emission ratio, since we combine a variety of natural gas composition measurements for wet and dry basins. We calculate a global literature emission ratio using hydrocarbon and dry natural gas production data from the top 5 producing natural gas basins around the world that made up 50% of the total natural gas production in 2019.[28,29] We also calculate a U.S. literature emission ratio using the top 7 natural-gas-producing basins that account for 86% of total U.S. natural gas production.[30,31] We show the relative production of the top global and U.S. basins used in our analysis in Figure S3. Additional summary statistics and sources for the composition measurements are included in Tables S4 and S5.

Separately, we calculate an "observationally informed emission ratio (OIER)" by taking the ratio between our revised C_3H_8 emissions with literature estimates of CH_4 emissions from oil and natural gas processes. The OIER for C_2H_6/CH_4 is calculated similarly. Previous studies have constrained global CH_4 emissions from natural gas/petroleum systems to range from 63 to 91 Tg/year.[25,32−37] Given our estimate for revised C_2H_6 and C_3H_8 emissions, this implies a mean alkane ratio of 100:[8.0,10.0]:[6.5, 7.3] molar % (CH_4/C_2H_6/C_3H_8) in 2016−2018. We compare our literature ratio with several OIER using global estimates in Figure 6 and with U.S. estimates in Figure S63. The small abundance of spatial and temporal literature measurements of raw gas composition throughout basins most affect the final uncertainty in the emission ratio comparison.

Unprocessed dry gas has a smaller C_3H_8/CH_4 and C_2H_6/CH_4 ratio compared to unprocessed associated gas from oil-producing basins ("wet" gas). A greater contribution of emissions from dry basins would decrease the magnitude of the overall literature ratio, assuming minimal C_3H_8 leakage after separation from raw gas, given the high market value of C_3H_8. In the U.S., the basin with the highest gas production is the Appalachian (East Coast) (Figure S3). If CH_4 leaks were proportional to production, we would expect a "dry" (small) emission ratio that resembles the composition of the Appalachian region (6% mass/mass of C_3H_8/CH_4, calculated from Table S5). However, we find the production-weighted literature ratio to be much larger than expected (15% mass/mass for C_3H_8/CH_4, Figure S63). The second-largest gas-producing region, the Permian (Southwestern U.S.), is also the largest oil producer in the U.S. and vastly overpowers the Appalachian in terms of oil production (Figure S3). The magnitude of our production-weighted raw gas "literature" emission ratios suggest a significant contribution from wet gas and emissions that are biased toward oil-producing basins. We find similar results for global emission ratios (Figure 6).

The Global Carbon Project CH_4 emissions estimate implies an OIER that is dry relative to the production-weighted raw gas ratio (literature ratio) (Figure 6). Instead, the IEA (76 Tg/year) and Scarpelli et al. (66 Tg/year) CH_4 emission estimates

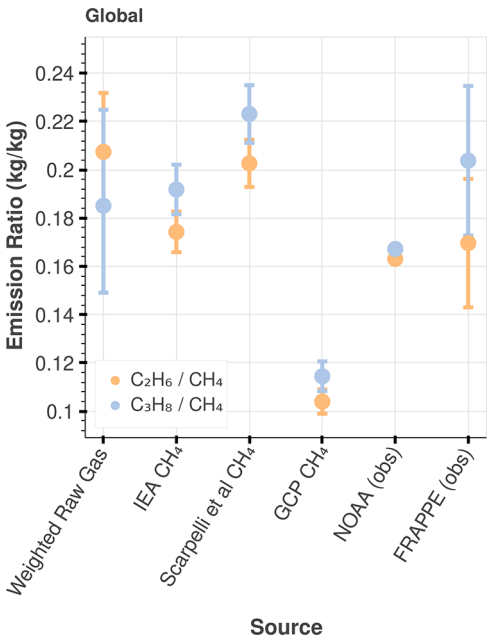

Figure 6. Global literature and observationally informed emission ratios (OIER) C_3H_8/CH_4 and C_2H_6/CH_4. The "weighted raw gas ratio" in the figure represents the "literature ratio" described in the text, calculated using eq 2. OIER, ratios between our revised C_2H_6 and C_3H_8 emissions and literature CH_4 emission estimates, are shown for several literature CH_4 estimates, including IEA (76.4 Tg/year),[34] Scarpelli et al. (65.7 Tg/year),[33] and Global Carbon Project bottom-up estimate (128 Tg/year, 2008−2017 average).[32] The variability in the literature ratio is attributed to the 95% CI of pairs bootstrap samples of hydrocarbon composition measurements (see text for more detail). The variability in the OIER is attributed to the 95% CI of our revised C_3H_8 and C_2H_6 emission estimates. We also compare C_3H_8/CH_4 and C_2H_6/CH_4 correlations from in situ observations, including NOAA observations from Northern Oklahoma (2017 average from Figure S21, units of kg/kg) and FRAPPE observations from Northern Colorado (2014 from Figure S9, units of kg/kg). The variability in the NOAA ratio is relatively low because it is calculated from a multiyear average slope, and the error in the slope is low (see Figure S21, left). The variability in the FRAPPE ratio is relatively high because we use the 95% CI derived directly from our bootstrap samples, as described in the Materials and Methods section.

yield an OIER that is within a few percent of the production-weighted raw gas literature ratio, given our revised C_3H_8 and C_2H_6 emissions. Both of those studies estimate oil production emissions to have a relatively higher contribution to the global footprint compared to dry gas production.

The FRAPPE and NOAA Oklahoma observed emission ratios compare well to the global OIER (Figure 6) and U.S. OIER (Figure S63), suggesting high emissions from oil production. Indeed, there are substantial oil production activities (Figures S15−S18) surrounding the NOAA Oklahoma and FRAPPE observation sites. Increasing trends in the Oklahoma emission ratios are consistent with production trends: oil production in Oklahoma tripled from 2010 to 2017[38,39] (compared to doubling of gas production), and in 2020, Oklahoma was the fourth-largest oil producer in the U.S.[40] (Note that Oklahoma was not included in calculations for the literature ratio, since Oklahoma natural gas production does not rank in the top 7.) Several factors may reduce incentive or the ability for oil producers to capture associated

https://doi.org/10.1021/acs.est.2c00927
Environ. Sci. Technol. 2022, 56, 9623−9631

natural gas byproducts, including low market prices and lagging pipeline infrastructure.[41]

Since our findings suggest that CH_4 losses are likely greater and biased toward oil-producing sites, a significant fraction of bottom-up estimates of CH_4 emissions may be misallocated to dry CH_4 production when they should instead be included with the oil production sector. Correctly attributing CH_4 emissions to oil production would increase the greenhouse gas footprint of petroleum-based transportation, while decreasing the greenhouse gas emissions ascribed to natural-gas-powered power plants. At a minimum, the CO_2 equivalent footprint of the global transportation sector would increase by roughly 5%, using IEA's estimate of 76 Tg/year CH_4 emissions from oil and natural gas and recent transportation CO_2 emission estimates (section 6.2, SI).[36,42] This estimate will only increase when accounting for vented and flared losses of associated natural gas that is not accounted for in marketed associated gas (which we use to calculate these numbers).

■ ASSOCIATED CONTENT

Supporting Information

The Supporting Information is available free of charge at https://pubs.acs.org/doi/10.1021/acs.est.2c00927.

U.S. and global economic and production trends of oil and natural gas; statistical methods and chemical aging approach to NOAA and FRAPPE observations; methane anomaly determination for NOAA and FRAPPE observations; yearly methane anomaly ratios for NOAA observations; ATom and HIPPO aircraft campaign filtering methods; GEOS-Chem simulation results after revising propane emissions; Bayesian inference results; emission ratio calculation details; analysis of reallocating methane emissions to the transportation sector (PDF)

■ AUTHOR INFORMATION

Corresponding Author

Paul O. Wennberg − *Division of Engineering and Applied Science and Division of Geological and Planetary Sciences, California Institute of Technology, Pasadena, California 91125, United States;* orcid.org/0000-0002-6126-3854; Email: wennberg@caltech.edu

Authors

Ariana L. Tribby − *Division of Chemistry and Chemical Engineering, California Institute of Technology, Pasadena, California 91125, United States;* orcid.org/0000-0002-6435-4575

Justin S. Bois − *Division of Biology and Biological Engineering, California Institute of Technology, Pasadena, California 91125, United States*

Stephen A. Montzka − *National Oceanic and Atmospheric Administration, Global Monitoring Laboratory, Boulder, Colorado 80305, United States*

Elliot L. Atlas − *Rosenstiel School of Marine and Atmospheric Science, University of Miami, Miami, Florida 33149, United States;* orcid.org/0000-0003-3847-5346

Isaac Vimont − *National Oceanic and Atmospheric Administration, Global Monitoring Laboratory, Boulder, Colorado 80305, United States; Cooperative Institute for Research in Environmental Sciences, University of Colorado Boulder, Boulder, Colorado 80309, United States*

Xin Lan − *National Oceanic and Atmospheric Administration, Global Monitoring Laboratory, Boulder, Colorado 80305, United States; Cooperative Institute for Research in Environmental Sciences, University of Colorado Boulder, Boulder, Colorado 80309, United States*

Pieter P. Tans − *National Oceanic and Atmospheric Administration, Global Monitoring Laboratory, Boulder, Colorado 80305, United States*

James W. Elkins − *National Oceanic and Atmospheric Administration, Global Monitoring Laboratory, Boulder, Colorado 80305, United States; Cooperative Institute for Research in Environmental Sciences, University of Colorado Boulder, Boulder, Colorado 80309, United States;* orcid.org/0000-0003-4701-3100

Donald R. Blake − *Department of Chemistry, University of California—Irvine, Irvine, California 92697, United States*

Complete contact information is available at: https://pubs.acs.org/10.1021/acs.est.2c00927

Notes

The authors declare no competing financial interest.

■ ACKNOWLEDGMENTS

This work was supported by the Resnick Sustainability Institute, including computations conducted in the Resnick High Performance Computing Center. A.L.T. received funding from NSF Award No. DGE-1745301. NOAA support was provided for HIPPO by NSF Award No. AGS-0628452; California Institute of Technology support for ATom was provided by NASA Grant Award No. NNX15AG61A. NOAA support for ATom was provided by NASA EVS2 Award No. NNH17AE26I; additional support was provided by NASA Upper Atmosphere Research Program award No. NNH13A-V69I. NOAA laboratory and salary support is from NOAA Climate Change Program. S.A.M. acknowledges funding in part from NOAA Climate Program Office's AC4 Program. NOAA flask sampling and technical support was provided by Dr. Fred Moore of NOAA/CIRES. Additional technical support was provided by C. Siso, B. Miller, M. Crotwell, C. Sweeney, A. Andrews, J. Higgs, D. Neff, J. Kofler, K. McKain, M. Madronich, P. Handley, and S. Wolter. We thank IHS Markit for providing PointLogic economic data.

■ REFERENCES

(1) U.S. Energy Information Administration. *Where our natural gas comes from*; https://www.eia.gov/energyexplained/natural-gas/where-our-natural-gas-comes-from.php (accessed 2022-03-18).

(2) Lan, X.; Tans, P.; Sweeney, C.; Andrews, A.; Dlugokencky, E.; Schwietzke, S.; Kofler, J.; McKain, K.; Thoning, K.; Crotwell, M.; Montzka, S.; Miller, B. R.; Biraud, S. C. Long-Term Measurements Show Little Evidence for Large Increases in Total U.S. Methane Emissions Over the Past Decade. *Geophys. Res. Lett.* **2019**, *46* (9), 4991−4999.

(3) Turner, A. J.; Frankenberg, C.; Wennberg, P. O.; Jacob, D. J. Ambiguity in the Causes for Decadal Trends in Atmospheric Methane and Hydroxyl. *Proc. Natl. Acad. Sci. U. S. A.* **2017**, *114* (21), 5367−5372.

(4) Kort, E. A.; Smith, M. L.; Murray, L. T.; Gvakharia, A.; Brandt, A. R.; Peischl, J.; Ryerson, T. B.; Sweeney, C.; Travis, K. Fugitive Emissions from the Bakken Shale Illustrate Role of Shale Production in Global Ethane Shift: Ethane Emissions From the Bakken Shale. *Geophys. Res. Lett.* **2016**, *43* (9), 4617−4623.

(5) U.S. Energy Information Administration. *Hydrocarbon gas liquids explained*; https://www.eia.gov/energyexplained/hydrocarbon-gas-

liquids/prices-for-hydrocarbon-gas-liquids.php (accessed 2022-01-31).
(6) Wofsy, S. C. HIAPER Pole-to-Pole Observations (HIPPO): Fine-Grained, Global-Scale Measurements of Climatically Important Atmospheric Gases and Aerosols. *Philos. Trans. R. Soc. Math. Phys. Eng. Sci.* **2011**, *369* (1943), 2073−2086.
(7) Thompson, C. R.; Wofsy, S. C.; Prather, M. J.; Newman, P. A.; Hanisco, T. F.; Ryerson, T. B.; Fahey, D. W.; Apel, E. C.; Brock, C. A.; Brune, W. H.; Froyd, K.; Katich, J. M.; Nicely, J. M.; Peischl, J.; Ray, E.; Veres, P. R.; Wang, S.; Allen, H. M.; Asher, E.; Bian, H.; Blake, D.; Bourgeois, I.; Budney, J.; Bui, T. P.; Butler, A.; Campuzano-Jost, P.; Chang, C.; Chin, M.; Commane, R.; Correa, G.; Crounse, J. D.; Daube, B.; Dibb, J. E.; DiGangi, J. P.; Diskin, G. S.; Dollner, M.; Elkins, J. W.; Fiore, A. M.; Flynn, C. M.; Guo, H.; Hall, S. R.; Hannun, R. A.; Hills, A.; Hintsa, E. J.; Hodzic, A.; Hornbrook, R. S.; Huey, L. G.; Jimenez, J. L.; Keeling, R. F.; Kim, M. J.; Kupc, A.; Lacey, F.; Lait, L. R.; Lamarque, J.-F.; Liu, J.; McKain, K.; Meinardi, S.; Miller, D. O.; Montzka, S. A.; Moore, F. L.; Morgan, E. J.; Murphy, D. M.; Murray, L. T.; Nault, B. A.; Neuman, J. A.; Nguyen, L.; Gonzalez, Y.; Rollins, A.; Rosenlof, K.; Sargent, M.; Schill, G.; Schwarz, J. P.; Clair, J. M. St.; Steenrod, S. D.; Stephens, B. B.; Strahan, S. E.; Strode, S. A.; Sweeney, C.; Thames, A. B.; Ullmann, K.; Wagner, N.; Weber, R.; Weinzierl, B.; Wennberg, P. O.; Williamson, C. J.; Wolfe, G. M.; Zeng, L. The NASA Atmospheric Tomography (ATom) Mission: Imaging the Chemistry of the Global Atmosphere. *Bull. Am. Meteorol. Soc.* **2022**, *103* (3), E761−E790.
(8) Mund, J.; Thoning, K.; Tans, P.; Dlugokencky, E. *NOAA ESRL/GMD Annual Period of Record Operational Carbon Cycle & Greenhouse Gases (CCGGs) from Surface Stations* **2017**, DOI: 10.7289/V5CN725S.
(9) Mund, J.; Thoning, K.; Tans, P.; Andrews, A.; Kofler, J.; Trudeau, M. E.; Bakwin, P. S.; Fisher, M. L.; Sweeney, C.; Desai, A. R. *Earth System Research Laboratory Carbon Cycle and Greenhouse Gases Group Continuous Measurements of CO2, CO, and CH4 from Tall Towers* **2017**, DOI: 10.7289/V57W69F2.
(10) Mund, J.; Thoning, K.; Tans, P.; Sweeny, C.; Higgs, J.; Wolter, S.; Crotwell, A.; Neff, D.; Dlugokencky, E.; Lang, P.; Novelli, P.; Moglia, E.; Crotwell, M. *Earth System Research Laboratory Carbon Cycle and Greenhouse Gases Group Flask-Air Sample Measurements of CO2, CH4, CO, N2O, H2, and SF6 from the Aircraft Program* **2017**, DOI: 10.7289/V5N58JMF.
(11) Vimont, I.; Montzka, S.; Hall, B.; Siso, C.; Crotwell, M. *Preliminary Ethane and Propane Data Used in Tribby et al.*; https://gml.noaa.gov/ccgg/arc/?id=155 (accessed 2022-05-27).
(12) Andrews, A. E.; Kofler, J. D.; Trudeau, M. E.; Williams, J. C.; Neff, D. H.; Masarie, K. A.; Chao, D. Y.; Kitzis, D. R.; Novelli, P. C.; Zhao, C. L.; Dlugokencky, E. J.; Lang, P. M.; Crotwell, M. J.; Fischer, M. L.; Parker, M. J.; Lee, J. T.; Baumann, D. D.; Desai, A. R.; Stanier, C. O.; De Wekker, S. F. J.; Wolfe, D. E.; Munger, J. W.; Tans, P. P. CO2, CO, and CH4Measurements from Tall Towers in the NOAA Earth System Research Laboratory's Global Greenhouse Gas Reference Network: Instrumentation, Uncertainty Analysis, and Recommendations for Future High-Accuracy Greenhouse Gas Monitoring Efforts. *Atmospheric Meas. Technol.* **2014**, *7* (2), 647−687.
(13) Sweeney, C.; Karion, A.; Wolter, S.; Newberger, T.; Guenther, D.; Higgs, J. A.; Andrews, A. E.; Lang, P. M.; Neff, D.; Dlugokencky, E.; Miller, J. B.; Montzka, S. A.; Miller, B. R.; Masarie, K. A.; Biraud, S. C.; Novelli, P. C.; Crotwell, M.; Crotwell, A. M.; Thoning, K.; Tans, P. P. Seasonal Climatology of CO_2 across North America from Aircraft Measurements in the NOAA/ESRL Global Greenhouse Gas Reference Network: VERTICAL CLIMATOLOGY OF CO_2 IN NA. *J. Geophys. Res. Atmospheres* **2015**, *120* (10), 5155−5190.
(14) Jacob, D. J. *Introduction to Atmospheric Chemistry*; Princeton University Press: Princeton, NJ, 1999; pp 52−53.
(15) Seinfeld, J. H.; Pandis, S. N. *Atmospheric Chemistry and Physics: From Air Pollution to Climate Change*, 3rd ed.; John Wiley & Sons: Hoboken, NJ, 2016; p 129.
(16) Keppel-Aleks, G.; Wennberg, P. O.; Schneider, T. Sources of Variations in Total Column Carbon Dioxide. *Atmospheric Chem. Phys.* **2011**, *11* (8), 3581−3593.
(17) Keppel-Aleks, G.; Wennberg, P. O.; Washenfelder, R. A.; Wunch, D.; Schneider, T.; Toon, G. C.; Andres, R. J.; Blavier, J.-F.; Connor, B.; Davis, K. J.; Desai, A. R.; Messerschmidt, J.; Notholt, J.; Roehl, C. M.; Sherlock, V.; Stephens, B. B.; Vay, S. A.; Wofsy, S. C. The Imprint of Surface Fluxes and Transport on Variations in Total Column Carbon Dioxide. *Biogeosciences* **2012**, *9* (3), 875−891.
(18) Wohltmann, I. Integrated Equivalent Latitude as a Proxy for Dynamical Changes in Ozone Column. *Geophys. Res. Lett.* **2005**, *32* (9), DOI: 10.1029/2005GL022497.
(19) Parrish, D. D.; Stohl, A.; Forster, C.; Atlas, E. L.; Blake, D. R.; Goldan, P. D.; Kuster, W. C.; de Gouw, J. A. Effects of Mixing on Evolution of Hydrocarbon Ratios in the Troposphere: MIXING EFFECTS ON NMHC RATIO EVOLUTION. *J. Geophys. Res. Atmospheres* **2007**, *112* (D10), DOI: 10.1029/2006JD007583.
(20) Department of Energy. *Liquefied Natural Gas: Understanding the Basic Facts*; DOE/FE-0489; United States of America, 2005.
(21) Rutherford, J. S.; Sherwin, E. D.; Ravikumar, A. P.; Heath, G. A.; Englander, J.; Cooley, D.; Lyon, D.; Omara, M.; Langfitt, Q.; Brandt, A. R. Closing the Methane Gap in US Oil and Natural Gas Production Emissions Inventories. *Nat. Commun.* **2021**, *12* (1), 4715.
(22) National Oceanic and Atmospheric Administration (NOAA). *The Science behind the Polar Vortex: You Might Want to Put on a Sweater*, 2021.
(23) Dalsøren, S. B.; Myhre, G.; Hodnebrog, Ø.; Myhre, C. L.; Stohl, A.; Pisso, I.; Schwietzke, S.; Höglund-Isaksson, L.; Helmig, D.; Reimann, S.; Sauvage, S.; Schmidbauer, N.; Read, K. A.; Carpenter, L. J.; Lewis, A. C.; Punjabi, S.; Wallasch, M. Discrepancy between Simulated and Observed Ethane and Propane Levels Explained by Underestimated Fossil Emissions. *Nat. Geosci.* **2018**, *11* (3), 178−184.
(24) Helmig, D.; Rossabi, S.; Hueber, J.; Tans, P.; Montzka, S. A.; Masarie, K.; Thoning, K.; Plass-Duelmer, C.; Claude, A.; Carpenter, L. J.; Lewis, A. C.; Punjabi, S.; Reimann, S.; Vollmer, M. K.; Steinbrecher, R.; Hannigan, J. W.; Emmons, L. K.; Mahieu, E.; Franco, B.; Smale, D.; Pozzer, A. Reversal of Global Atmospheric Ethane and Propane Trends Largely Due to US Oil and Natural Gas Production. *Nat. Geosci.* **2016**, *9* (7), 490−495.
(25) Höglund-Isaksson, L. Bottom-up Simulations of Methane and Ethane Emissions from Global Oil and Gas Systems 1980 to 2012. *Environ. Res. Lett.* **2017**, *12* (2), 024007.
(26) Franco, B.; Mahieu, E.; Emmons, L. K.; Tzompa-Sosa, Z. A.; Fischer, E. V.; Sudo, K.; Bovy, B.; Conway, S.; Griffin, D.; Hannigan, J. W.; Strong, K.; Walker, K. A. Evaluating Ethane and Methane Emissions Associated with the Development of Oil and Natural Gas Extraction in North America. *Environ. Res. Lett.* **2016**, *11* (4), 044010.
(27) Simpson, I. J.; Sulbaek Andersen, M. P.; Meinardi, S.; Bruhwiler, L.; Blake, N. J.; Helmig, D.; Rowland, F. S.; Blake, D. R. Long-Term Decline of Global Atmospheric Ethane Concentrations and Implications for Methane. *Nature* **2012**, *488* (7412), 490−494.
(28) International Energy Agency. *IEA Atlas of Energy: Natural Gas Production*; http://energyatlas.iea.org/#!/tellmap/-1165808390 (accessed 2022-05-27).
(29) International Energy Agency. *IEA Atlas of Energy: Crude Oil Production*; http://energyatlas.iea.org/#!/tellmap/-1920537974 (accessed 2022-05-27).
(30) U.S. Energy Information Administration. *Drilling Productivity Report for Key Tight Oil and Shale Gas Regions*, https://www.eia.gov/petroleum/drilling/ (accessed 2022-05-27).
(31) Worldwide Power Products. *10 Biggest Shale Plays in the US - New & Used Generators, Ends and Engines*; Worldwide Power Products: Houston, TX.
(32) Saunois, M.; Stavert, A. R.; Poulter, B.; Bousquet, P.; Canadell, J. G.; Jackson, R. B.; Raymond, P. A.; Dlugokencky, E. J.; Houweling, S.; Patra, P. K.; Ciais, P. Global Methane Budget 2000−2017. *Earth Syst. Sci. Data* **2020**, *12*, 1561−1623.

(33) Scarpelli, T. R.; Jacob, D. J.; Maasakkers, J. D.; Sulprizio, M. P.; Sheng, J.-X.; Rose, K.; Romeo, L.; Worden, J. R.; Janssens-Maenhout, G. A Global Gridded (0.1° × 0.1°) Inventory of Methane Emissions from Oil, Gas, and Coal Exploitation Based on National Reports to the United Nations Framework Convention on Climate Change. *Earth Syst. Sci. Data* **2020**, *12* (1), 563−575.
(34) IEA. *Methane Tracker Database: Interactive Database of Country and Regional Estimates for Methane Emissions and Abatement Options*; https://www.iea.org/articles/methane-tracker-data-explorer (accessed 2022-05-27).
(35) Maasakkers, J. D.; Jacob, D. J.; Sulprizio, M. P.; Turner, A. J.; Weitz, M.; Wirth, T.; Hight, C.; DeFigueiredo, M.; Desai, M.; Schmeltz, R.; Hockstad, L.; Bloom, A. A.; Bowman, K. W.; Jeong, S.; Fischer, M. L. Gridded National Inventory of U.S. Methane Emissions. *Environ. Sci. Technol.* **2016**, *50* (23), 13123−13133.
(36) EPA (Environmental Protection Agency). *Global Anthropogenic Non-CO2 Greenhouse Gas Emissions: 1990−2030*; https://www.epa.gov/global-mitigation-non-co2-greenhouse-gases/global-non-co2-ghg-emissions-1990-2030 (accessed 2022-05-27).
(37) Turner, A. J.; Jacob, D. J.; Wecht, K. J.; Maasakkers, J. D.; Lundgren, E.; Andrews, A. E.; Biraud, S. C.; Boesch, H.; Bowman, K. W.; Deutscher, N. M.; Dubey, M. K.; Griffith, D. W. T.; Hase, F.; Kuze, A.; Notholt, J.; Ohyama, H.; Parker, R.; Payne, V. H.; Sussmann, R.; Sweeney, C.; Velazco, V. A.; Warneke, T.; Wennberg, P. O.; Wunch, D. Estimating Global and North American Methane Emissions with High Spatial Resolution Using GOSAT Satellite Data. *Atmospheric Chem. Phys.* **2015**, *15* (12), 7049−7069.
(38) U.S. Energy Information Administration. *Petroleum & Other Liquids: Oklahoma Field Production of Crude Oil*; https://www.eia.gov/dnav/pet/hist/LeafHandler.ashx?f=M&=PET&=MCRFPOK1 (accessed 2022-05-27).
(39) U.S. Energy Information Administration. *Natural Gas: Oklahoma Natural Gas Marketed Production*; https://ycharts.com/indicators/us_natural_gas_marketed_production_ngm#:~:text=US%20Natural%20Gas%20Marketed%20Production%20is%20at%20a%20current%20level,2.586T%20one%20year%20ago. (accessed 2022-05-27).
(40) U.S. Energy Information Administration. *Oklahoma State Profile Analysis*, 2021.
(41) Crowley, K.; Collins, R. Oil Producers Are Burning Enough "Waste" Gas to Power Every Home in Texas. *Bloomberg* April 10, **2019**; https://www.bqprime.com/business/permian-basin-is-flaring-more-gas-than-texas-residents-use-daily.
(42) Liu, Z.; Ciais, P.; Deng, Z.; Lei, R.; Davis, S. J.; Feng, S.; Zheng, B.; Cui, D.; Dou, X.; Zhu, B.; Guo, R.; Ke, P.; Sun, T.; Lu, C.; He, P.; Wang, Y.; Yue, X.; Wang, Y.; Lei, Y.; Zhou, H.; Cai, Z.; Wu, Y.; Guo, R.; Han, T.; Xue, J.; Boucher, O.; Boucher, E.; Chevallier, F.; Tanaka, K.; Wei, Y.; Zhong, H.; Kang, C.; Zhang, N.; Chen, B.; Xi, F.; Liu, M.; Bréon, F.-M.; Lu, Y.; Zhang, Q.; Guan, D.; Gong, P.; Kammen, D. M.; He, K.; Schellnhuber, H. J. Near-Real-Time Monitoring of Global CO2 Emissions Reveals the Effects of the COVID-19 Pandemic. *Nat. Commun.* **2020**, *11* (1), 5172.

https://doi.org/10.1021/acs.est.2c00927
Environ. Sci. Technol. 2022, 56, 9623−9631